Molecular Cancer Therapeutics

Hsp90 Inhibitor–Mediated Disruption of Chaperone Association of ATR with Hsp90 Sensitizes Cancer Cells to DNA Damage

Kyungsoo Ha[1], Warren Fiskus[2], Rekha Rao[2], Ramesh Balusu[2], Sreedhar Venkannagari[2], Narasimha Rao Nalabothula[2], and Kapil N. Bhalla[2]

Abstract

Following DNA damage that results in stalled replication fork, activation of ATR-CHK1 signaling induces the DNA damage response (DDR) in transformed cells. In the present studies on human cervical and breast cancer cells, we determined the effects of hsp90 inhibition on the levels and accumulation of DNA damage/repair–associated proteins following exposure to γ-ionizing radiation (IR; 4 Gy). We show that hsp90 inhibition with 17-allylamino-demehoxygeldanamycin or the novel, nongeldanamycin analogue AUY922 (resorcinylic isoxazole amide; Novartis Pharma) dose-dependently reduced the levels of ATR and CHK1 without affecting ATM levels. AUY922-mediated depletion of ATR and CHK1 was associated with an increase in their polyubiquitylation and decreased binding to hsp90. Cotreatment with bortezomib partially restored AUY922-mediated depletion of ATR and CHK1 levels. Additionally, treatment with AUY922 reduced the accumulation of ATR, p53BP1, and CHK1 but not γ-H2AX to the sites of DNA damage. Following exposure to IR, AUY922 treatment abrogated IR-induced phospho (p)-ATR and p-CHK1 levels, but significantly enhanced γ-H2AX levels. AUY922 treatment also increased IR-induced accumulation of the cells in G_2–M phase of the cell cycle, inhibited the repair of IR-induced DNA damage, and augmented IR-mediated loss of clonogenic survival. Short hairpin RNA–mediated depletion of ATR also inhibited IR-induced p-ATR and p-CHK1, but increased γ-H2AX levels, sensitizing cancer cells to IR-induced apoptosis and loss of clonogenic survival. These findings indicate that ATR is a bona fide hsp90 client protein and post-IR administration of AUY922, by inhibiting ATR-CHK1–mediated DDR, sensitizes cancer cells to IR. *Mol Cancer Ther; 10(7); 1194–206. ©2011 AACR.*

Introduction

DNA damage caused by environmental mutagens or reactive metabolic byproducts induces DNA damage response (DDR), which regulates cell-cycle transit, DNA repair, and apoptosis (1–3). DDR involves the phosphorylation and activation of 2 members of the phosphoinositide 3-kinase–related kinase (PIKK) family of protein kinases, ataxia telangiectasia mutated (ATM) and ATM and RAD3-related (ATR) proteins (3, 4). ATM is activated in response to the uncommon event of double-strand breaks (DSB), whereas ATR is activated in response to many different types of DNA damage, including single-strand breaks (SSB), base adducts, cross-links, and stalled replication forks (3, 4). ATR is activated when stalled replication forks result during replication of damaged DNA due to bulky adducts, SSBs, or DSBs (3, 4). ATR is essential for the viability of replicating human and mouse cells, whereas ATM is not (5, 6). At SSB and stalled replication forks, replication protein A coats the single-strand DNA and recruits ATR-interacting protein (ATRIP), which binds ATR and is essential for its stability (7). ATR activation in the ATR–ATRIP complex requires colocalization with the RAD9–RAD1–HUS1 complex (also called 9-1-1 complex), and recruitment of topoisomerase binding protein 1 (TOPBP1) to the complex (8, 9). During DDR triggered by UV, γ-ionizing radiation (IR), or hyperoxia, once the ATR-ATRIP–based complex is assembled at the stalled replication fork or a DNA lesion, activated ATR phosphorylates numerous substrates involved in cell-cycle checkpoint control, DNA repair, and apoptosis (3, 4). Notably, ATR phosphorylates and activates CHK1 (on Ser345 and Ser317; refs. 3, 4, 10). Active CHK1 phosphorylates CDC25 phosphatases, especially CDC25A (on Ser123) and CDC25C (on

Authors' Affiliations: [1]Medical College of Georgia, Augusta, Georgia and [2]The University of Kansas Cancer Center, Kansas City, Kansas

Note: Supplementary material for this article is available at Molecular Cancer Therapeutics Online (http://mct.aacrjournals.org/).

Corresponding Author: Kapil N. Bhalla, The University of Kansas Cancer Center, 3901 Rainbow Blvd., 4030 Robinson, MS 1027, Kansas City, KS 66160. Phone: 913-945-7086; Fax: 913-588-4701; E-mail: kbhalla@kumc.edu

doi: 10.1158/1535-7163.MCT-11-0094

Ser216), for ubiquitin-mediated degradation (11, 12). Therefore, CDC25A is unable to dephosphorylate and activate CDK2 and CDK1, leading to the cell-cycle arrest in the late G_1, S, and G_2 phases (13, 14). Collectively, these reported observations indicate that ATR is a master regulator of DDR, regulating cell-cycle transitions, DNA replication, and DNA repair. Recent studies have indicated that the stability of ATR and other PIKKs is dependent on the TEL2–TTI1–TTI2 (triple 2 complex), which has been reported to be associated with the hsp90 (15, 16). But the full characterization of the chaperone association of ATR with hsp90 as well as its significance for ATR stability and its role in DDR signaling induced in cancer cells by IR have not been carefully determined.

Heat shock protein 90 (hsp90) is an abundantly expressed and stress-inducible, homodimeric, ATP-dependent molecular chaperone (17). Hsp90 forms the core of a super chaperone machine, which has been shown to maintain a growing list of proteins, including signaling protein kinases, transcription factors, and other cytosolic or nuclear proteins (also known as hsp90 client proteins) into their functionally mature and active conformation (17, 18). ATP binding to the hydrophobic N-terminal pocket also alters hsp90 conformation, promoting the interaction of hsp90 with a set of cochaperones, which enables the folding of the metastable client proteins into their active conformation (17, 18). Previous reports have identified several DDR proteins, including CHK1, DNA-PK, FANCA, and BRCA2, as hsp90 client proteins such that hsp90 inhibition attenuates their levels and/or function (19–23). Among the reported hsp90 antagonists that are currently being investigated in clinical trials in various human malignancies are the geldanamycin and its analogue 17-allylamino-demehoxygeldanamycin (17-AAG), as well as the nongeldanamycin analogue AUY922 (17, 18, 24–26). These hsp90 antagonists bind to the N-terminal ATP-binding pocket of hsp90, replacing the nucleotide and inhibiting the chaperone function of hsp90 (17, 18, 24–26). For example, binding of AUY922 to hsp90 shifts it from a refolding chaperone complex to one that promotes degradation of client proteins (24–26). The misfolded client proteins are then directed to a covalent linkage with polyubiquitin by an E3 ubiquitin ligase, and subsequently degraded by the 26S proteasome (17, 18, 24–26). Therefore, hsp90 inhibitors can destabilize and deplete the client proteins involved in DDR, thereby inhibiting DNA repair and increasing the amount of damaged DNA, following treatment of transformed cells with IR, UV, or hyperoxia (20, 27, 28). Consistent with this, treatment with hsp90 inhibitor, for example, 17-AAG or AUY922, was shown to increase IR-induced γ-H2AX foci, a marker of DNA DSBs, inhibit the repair of damaged DNA, as well as sensitize transformed cells to IR (20, 27, 28). In the present studies, we show for the first time that in transformed cells ATR is a bona fide hsp90 client protein. We also show that treatment with hsp90 inhibitor attenuates the levels of both ATR and CHK1; and by inhibiting ATR-CHK1–mediated DDR signaling, hsp90 inhibitor treatment increases IR-mediated DNA damage and apoptosis of transformed cells.

Materials and Methods

Cell culture

The human cervical cancer cell line HeLa and human breast cancer cell line MCF-7 were obtained from American Type Culture Collection within 4 months of the experiments described in the following text. The cells were maintained in culture, as previously described (29, 30). MCF-7 cells were also cultured in serum-depleted condition (0.5% FBS) for 24 to 72 hours to induce growth arrest and determine its effects on ATR, DNA-PKcs, ATM, and mTOR levels (see the following text). HCT116 (colorectal cancer) and H1299 (non–small cell lung cancer) cells were maintained in McCoy's 5A and RPMI (containing 10% FBS, NEAA, and penicillin–streptomycin solution), respectively.

Reagents and antibodies

AUY922 was a gift from Novartis Pharmaceuticals Inc. 17-AAG was obtained from Developmental Therapeutics Branch of the Cancer Treatment Evaluation Program, National Cancer Institute, NIH (Bethesda, MD). Bortezomib was obtained from Millennium Pharmaceuticals. Cycloheximide (CHX) was purchased from Sigma-Aldrich. Anti–phospho (p)-ATR (S428) and anti-ATM antibodies were purchased from Cell Signaling Technology. Anti-CHK1, anti–p-CHK1 (S345), and anti-ubiquitin antibodies were purchased from Abcam. Anti-53BP1 antibody was purchased from Novus Biologicals and anti-ATR antibody was obtained from GeneTex. Anti-hsp90 and anti-hsp70 antibodies were purchased from StressGen Biotechnologies, and anti–γ-H2AX antibody was obtained from Millipore. Anti–β-actin antibody was purchased from Sigma-Aldrich.

DNA damage induction

HeLa and MCF-7 cells were irradiated by IR by using a ^{137}Cs source (Gamma cell 40 extractor; Nordion) or by microirradiation by using LSM510 META confocal microscope (Carl Zeiss) equipped with a pulsed Ti:Sapphire laser (800 nm, Mira 900; Coherent Inc.), as previously described (31). For the induction of replication stress, HeLa cells were treated with 10 mmol/L of hydroxyurea (HU; Sigma-Aldrich) for 2 hours. Then, cells were harvested or fixed for Western blot analyses or immunofluorescence staining for ATR, p-ATR, ATM, Chk1, 53BP1, and γ-H2AX.

RNA interference and transfection

For short hairpin RNA (shRNA)-mediated downregulation of ATR, HeLa cells were transiently transfected according to the manufacturer's instructions by using lipofectamine 2000 (Invitrogen) with the plasmid vectors expressing shRNA targeting human ATR or nonspecific

control (Santa Cruz Biotechnology), as previously described (30, 32). The cells were washed with media and incubated an additional 24 hours. Forty-eight hours after treatment with the vector or ATR shRNA, cells were treated with AUY922 or IR for Western blot or cell-cycle analyses.

Flow cytometric analysis

The flow cytometric evaluation of cell-cycle status and the percentage of cells in the G_1, S, and G_2–M phases were carried out according to a previously described method (33). Briefly, after drug treatment, cells were exposed to 4 Gy of IR and incubated for 8 to 16 hours at 37°C. Following this, cell-cycle status was determined by an Accuri CFlow6 flow cytometer (Accuri). For staining with p-histone H3 (Ser10) or γ-H2AX, cells were treated with 0.5% bovine serum albumin (BSA) for 10 minutes and incubated for 1 hour with Alexa 488–conjugated anti–p-histone H3 (Ser10), from Cell Signaling Technology, or 6 hours with Alexa 488–conjugated anti–γ-H2AX, from Cell Signaling Technology. Cells were washed with PBS, then stained with To-Pro3 iodide and analyzed by flow cytometry.

Clonogenic cell survival assays

Cells were treated with AUY922 for 16 hours followed by IR. After treatment, 300 cells were plated in triplicate and incubated at 37°C with 5% CO_2 for 10 days. At end of the incubation, colonies consisting of 50 or more cells in each well were counted and the surviving fraction was calculated by the formula: (mean number of colonies)/(number of cells seeded × plating efficiency). Plating efficiency was defined as the mean number of colonies divided by the number of cells seeded for unirradiated control cells (34).

Western blot analyses and immunoprecipitation

Western blot analyses were carried out on protein in the total cell lysates, as previously described (30, 35). For immunoprecipitation (IP), total cell lysates were mixed with anti-hsp90, anti-ATR, or anti-hsp70 antibody, and incubated overnight at 4°C with rotation. Protein G-agarose beads were added to the antibody–lysate mix and incubated for 3 hours. The beads were washed in lysis buffer (20 mmol/L Tris-HCl, 150 mmol/L NaCl, and 1% Triton X-100). Sample buffer was added and the immunoprecipitates were boiled before SDS-PAGE. Immunoblot analyses were carried out as previously described (30, 35). Densitometry was done by ImageQuant Version 5.2 (GE Healthcare).

RNA isolation and quantitative reverse transcription PCR

Total RNA was extracted from the cultured cells by using an RNAqueous-4PCR (Ambion) according to the manufacturer's protocol and converted into cDNA by using the High Capacity cDNA Reverse Transcription Kit (Applied Biosystems). Primers for amplification of ATR and CHK1 were purchased from Origene. Quantitative real-time PCR (RT-PCR) was carried out for ATR and CHK1 by using a StepOnePlus Real-Time PCR system (Applied Biosystems) and Power SYBR Green PCR Master Mix (Applied Biosystems), as previously described (30, 32). The PCRs were cycled 40 times after initial denaturation (95°C, 5 minutes) with the following parameters: denaturation at 95°C for 15 seconds; annealing at 60°C for 1 minute. Expression of glyceraldehyde-3-phosphate dehydrogenase (GAPDH) was used to normalize relative expression of the mRNA.

Immunofluorescence staining and confocal microscopy

HeLa and MCF-7 cells were grown on glass coverslides overnight at 37°C. Then cells were treated with AUY922 or IR to induce DNA damage and fixed with 4% paraformaldehyde and 0.5% Triton X-100 for 10 minutes. Following this, the slides were blocked with 3% BSA for 30 minutes and incubated with anti–p-ATR, anti–γ-H2AX, anti-ATR, anti-ubiquitin, anti-53BP1, anti-ATM, or anti-CHK1 antibody for 2 hours at 37°C. The slides were washed 3 times in 1× PBS and incubated with Alexa Fluor 594–or Alexa Fluor 488–conjugated secondary antibodies for 1 hour. After 3 washes with 1× PBS, the cells were counterstained by using SlowFade Gold antifade reagent with 4′,6-diamidino-2-phenylindole (DAPI; Invitrogen) and imaged by using a Zeiss LSM510 confocal microscope with a 63× 1.2 NA objective (Carl Zeiss), as previously described (30, 32).

Analysis of DNA damage repair by comet assay

These studies were conducted as previously described (20). Briefly, after treatment of AUY922 and IR, cells were harvested, mixed with low-melting agarose, and immediately poured onto glass slides. Slides were placed at 4°C in the dark for 10 minutes and immersed in prechilled lysis solution (Trevigen) for 30 minutes. Following this, slides were washed 3 times by immersing in 1 × Tris-borate EDTA buffer, and electrophoresis was done at 1 V/cm and 20 mA for 20 minutes. Then, slides were immersed in 70% ethanol for 5 minutes and stained with SYBR Green dye for 10 minutes (Trevigen). One hundred randomly selected cells per sample were captured under an Axioplan 2 fluorescent microscope (Carl Zeiss). The relative length and intensity of SYBR Green–stained DNA tails are proportional to the amount of DNA damage in the individual nuclei. Tail moment (tail length × percentage of DNA in the tail presenting DNA damage) is measured by TriTek Comet Score software (TriTek Corp.). Experiments were carried out in duplicate.

Statistical analyses

Data are expressed as mean ± SEM. Comparisons used Student's t test. P values less than 0.05 were assigned significance.

Results

Treatment with AUY922 inhibits radiation-induced cell survival, cell-cycle checkpoints, and DNA repair

We first determined the biological effects of a novel hsp90 inhibitor, AUY922, on IR-induced cell-cycle checkpoints and cell survival in cancer cells. Following exposure to IR, HeLa and MCF-7 cells were incubated for 16 hours in drug-free medium or exposed to 100 nmol/L AUY922 for 16 hours. Following this, cell-cycle analysis was carried out. Treatment with AUY922 alone increased the cell-cycle G_2–M phase accumulation, whereas exposure to IR induced G_1 phase accumulation in both cancer cell lines. Compared with treatment with AUY922 alone, cotreatment with AUY922 and IR abrogated IR-induced G_1 accumulation, and resulted in more G_2–M phase accumulation (Fig. 1A). Next, we determined the effect of AUY922 on IR-mediated loss of cell survival. Following exposure to AUY922 for 16 hours, cells were exposed to different doses of IR. Subsequently, the colony growth was evaluated after 10 days of culture in semisolid medium. Figure 1B shows that following treatment with AUY922, exposure to IR dose-dependently inhibited colony growth of HeLa and MCF-7 cells. Next, we determined the effect of AUY922 treatment on IR-induced DNA damage and repair at the individual cell level. Comet assays were carried out on HeLa cells 1, 8, or 16 hours after IR in control or AUY922 pretreated cells (Fig. 1C). Treatment with 100 nmol/L of AUY922 alone resulted in DNA fragmentation characterized by the appearance of comet tails. Although IR treatment induced the formation of the comet tails, the tail lengths

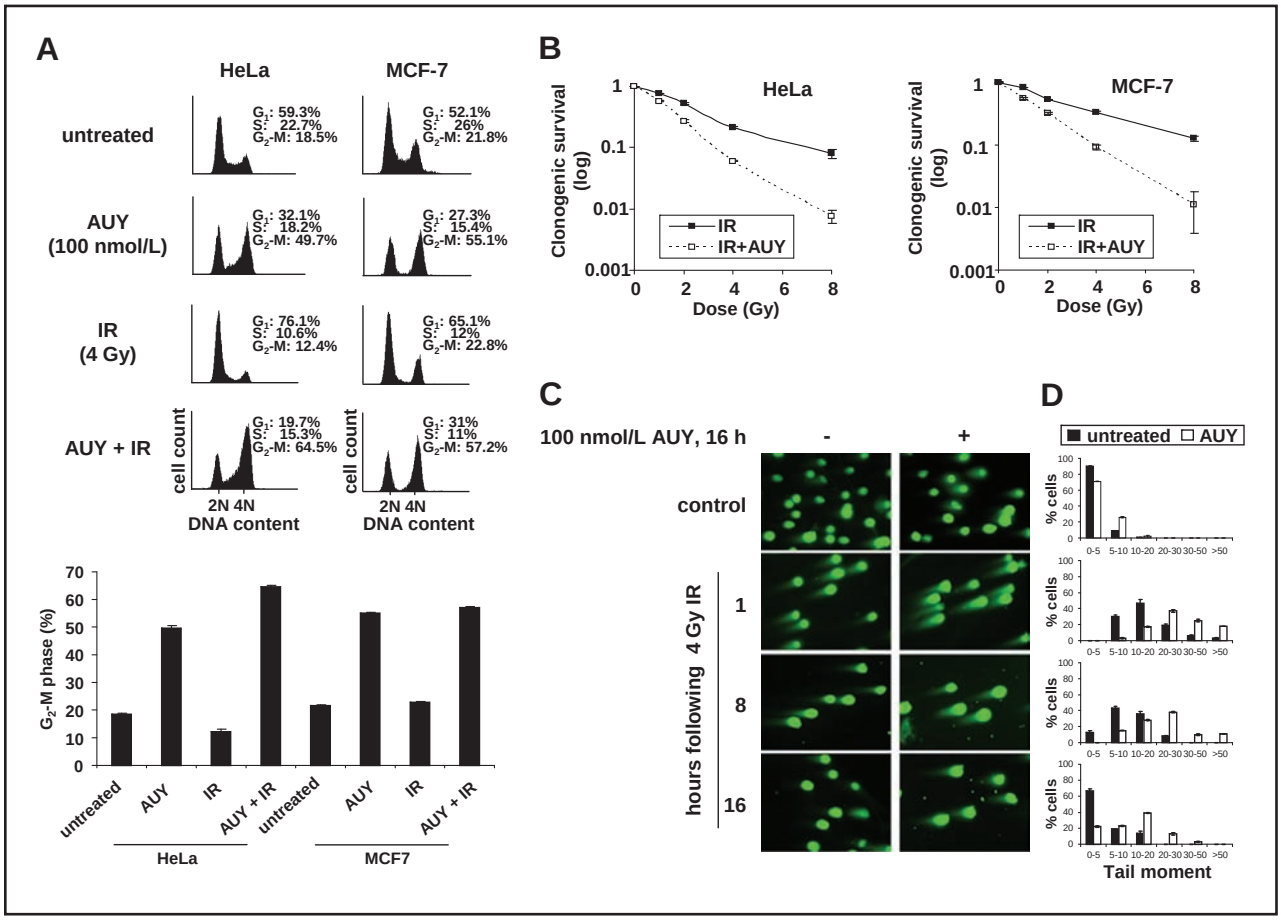

Figure 1. Treatment with AUY922 inhibits radiation-induced cell survival, cell-cycle checkpoints, and DNA repair. A, top, HeLa and MCF-7 cells were treated with 100 nmol/L AUY922 (AUY), 4 Gy of IR, or IR and 100 nmol/L of AUY for 16 hours. Cells receiving IR and/or IR + AUY were exposed to 4 Gy of IR, then incubated for 16 hours without or with 100 nmol/L of AUY. Following this, the cells were fixed and stained with propidium iodide. Cell-cycle analyses were carried out by flow cytometry. Bottom, graphic representation of the number of HeLa and MCF-7 cells in G_2–M following the indicated treatments. Columns represent the mean of 3 independent experiments; bars represent the SEM. B, HeLa cells were treated with 100 nmol/L of AUY for 16 hours. Then, the cells were exposed to the indicated doses of IR and 300 cells from each condition were plated in triplicate and cultured for 10 days. Values represent the mean percentage of colony growth of cells from each condition as a log% of control ± SEM. C and D, HeLa cells were treated with 100 nmol/L AUY for 16 hours and exposed to 4 Gy of IR. At the indicated times after IR, cells were analyzed by neutral comet assay. Representative images of cells (C) and the quantitative distribution of tail moments for 100 cells (D) for each time point are shown.

of the comets were longer in cells pretreated with AUY922 and then exposed to IR. This was estimated as the percentage of cells with longer tails or higher tail moment at the designated hours after IR treatment (Fig. 1D). When evaluated 16 hours after IR, while comet tails had attenuated in the untreated cells, AUY922 pretreated cells showed longer comet tails (Fig. 1C). This was estimated and represented as higher percentage of cells showing more tail moment at each of the time intervals after IR treatment in cells pretreated with AUY922. These results not only indicate higher DNA damage induced by IR but also inhibition of DNA damage repair in IR exposed cells that had been pretreated with AUY922 (Fig. 1C and D).

Treatment with AUY922 induces rapid depletion of ATR, p-ATR, and CHK1 expression levels

Next, we determined whether the evidence for higher DNA damage and attenuated DNA repair following IR in AUY922-treated cells was due to effects of hsp90 inhibition by AUY922 and depletion of the DDR signaling proteins. Exposure of HeLa and MCF-7 cells to AUY922 for 16 hours dose-dependently depleted the levels of p-ATR, ATR, and CHK1 levels, without significantly affecting the levels of ATM (Fig. 2A, top). Increasing exposure intervals to AUY922 had a similar effect on the p-ATR, ATR, and CHK1 levels in HeLa (Fig. 2B). Exposure of HeLa and MCF-7 cells to a different hsp90 inhibitor, that is, the geldanamycin analogue hsp90 inhibitor 17-AAG, also dose-dependently depleted p-ATR, ATR, and CHK1, but not ATM levels (Fig. 2A, bottom). Treatment with AUY922 caused a similar depletion of ATR, p-ATR, and CHK1 in HCT116 and H1299 cells (Supplementary Fig. S1). It is noteworthy that 24 to 48 hours following a washout of the drug after AUY922 treatment of HeLa cells (100 nmol/L for 16 hours), the levels of ATR, p-ATR, and CHK1 were completely restored (Fig. 2C). This suggests that in cells surviving after the AUY922 treatment, DDR response would also be restored due to repletion of the levels of p-ATR, ATR, and CHK1. We next determined the effect of AUY922 and/or IR on the mRNA levels of ATR and CHK1. As shown in

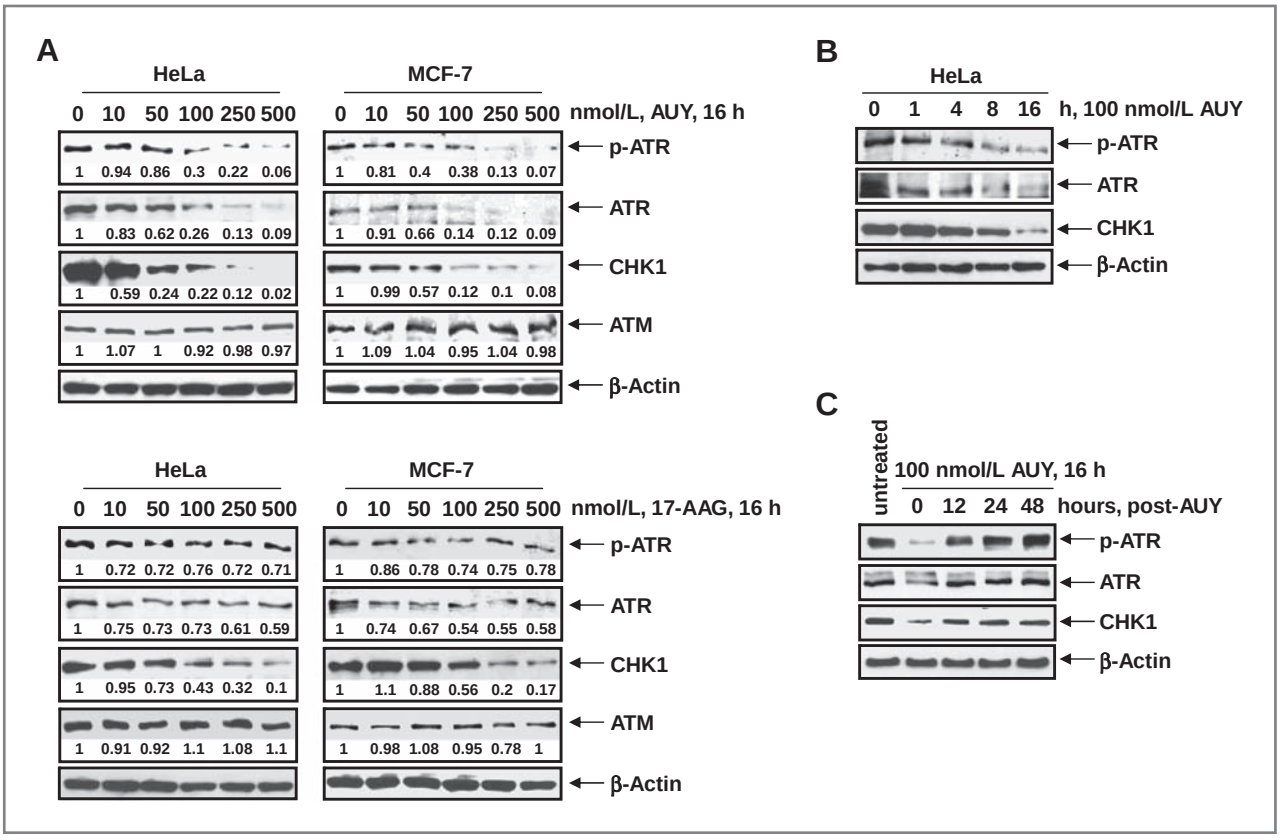

Figure 2. Treatment with AUY922 (AUY) induces rapid depletion of ATR, p-ATR, and CHK1 expression levels. A, HeLa and MCF-7 cells were treated with the indicated concentrations of AUY or 17-AAG for 16 hours. Following this, total cell lysates were prepared and immunoblot analyses were carried out for p-ATR (S428), ATR, CHK1, and ATM. The expression levels of β-actin in the lysates served as the loading control. B, HeLa cells were treated with 100 nmol/L AUY922 for the indicated times. At the end of treatment, total cell lysates were prepared and immunoblot analyses were carried out for p-ATR, ATR, and CHK1. The expression levels of β-actin in the lysates served as the loading control. C, HeLa cells were treated with 100 nmol/L AUY for 16 hours. Following treatment, cells were washed with 1× PBS and cultured in drug-free medium for the indicated times. Then, cell lysates were prepared and immunoblot analyses were carried out for p-ATR, ATR, and CHK1. The expression levels of β-actin in the lysates served as the loading control.

Fig. 3A, neither AUY922 nor IR treatment significantly affected the mRNA levels of ATR and CHK1 in HeLa cells.

Treatment with AUY922 inhibits the activation of ATR and CHK1 and increases γ-H2AX expression levels following IR

Treatment with an hsp90 inhibitor is known to result in the depletion of the half-life of hsp90 client proteins (32). Therefore, we determined the effect of AUY922 on the half-life of ATR and CHK1 in HeLa cells, by determining the effect on their expression levels over 16 hours of treatment with 100 μg/mL the protein synthesis inhibitor CHX alone versus cotreatment with CHX and AUY922 (Fig. 3B). As shown, treatment with CHX alone reduced the percentage of fractions remaining over 16 hours of both ATR and CHK1 proteins, which were further attenuated over 16 hours following cotreatment with AUY922 and CHX. This indicated that hsp90 promotes the stabilities of ATR and CHK1 proteins, and AUY922 treatment significantly decreased the half-life of ATR and CHK1. We next studied the effects of hsp90 inhibition on the phosphorylation and activation of ATR and CHK1 in response to DNA damage. Figure 3C shows that exposure to IR alone rapidly induced the levels of p-ATR and p-CHK1 over 16 hours, without significantly affecting the levels of ATR and CHK1. Post-IR treatment with AUY922 attenuated IR-induced p-ATR and p-CHK1 levels. It also inhibited the total ATR and CHK1 levels, 8 and 16 hours post-IR treatment. In contrast, post-IR AUY922 treatment further increased the γ-H2AX levels induced by exposure to IR (Fig. 3C). We also determined the effects of AUY922 on the activation of ATR in response to replicative stress induced by HU. The effect of AUY922 treatment on HU-mediated induction of p-ATR, p-CHK1, and γ-H2AX was evaluated in HeLa cells. The results shown in Supplementary Fig. S2 show that treatment with AUY922 abrogates HU-mediated increase in p-ATR and p-CHK1 levels, but the cotreatment caused greater accumulation of γ-H2AX.

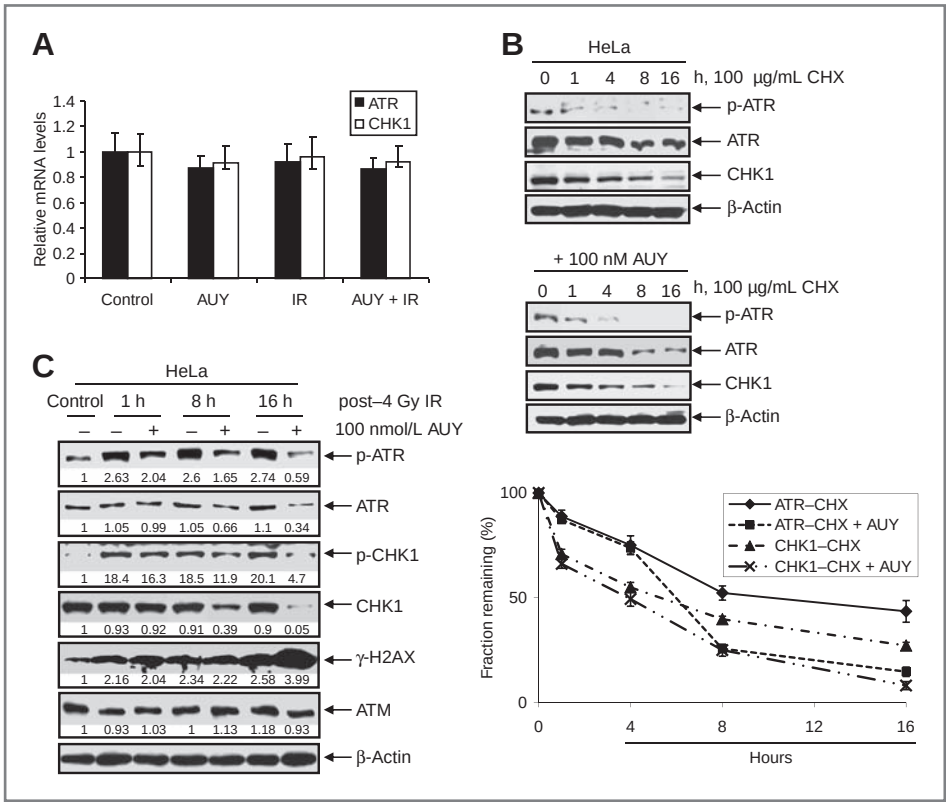

Figure 3. Treatment with AUY922 (AUY) inhibits the activation of ATR and CHK1 and increases γ-H2AX expression levels following IR. A, HeLa cells were treated with 100 nmol/L AUY, 4 Gy of IR, or IR and 100 nmol/L of AUY for 16 hours. Cells receiving IR and/or IR + AUY were exposed to 4 Gy of IR, then incubated for 16 hours without or with 100 nmol/L of AUY. Following this, total RNA was isolated and quantitative RT-PCR was carried out for ATR and CHK1. Expression levels were normalized against GAPDH. B, top, HeLa cells were treated with 100 μg/mL CHX and/or 100 nmol/L AUY for the indicated times. After treatment, cell lysates were prepared and immunoblot analyses were carried out for p-ATR, ATR, and CHK1. The expression levels of β-actin in the lysates served as the loading control. Bottom, quantification of p-ATR, ATR, and CHK1 expression following treatment with CHX and/or AUY922. Values represent the mean ± SEM from 3 independent experiments. C, HeLa cells were exposed to 4 Gy of IR, then immediately treated with 100 nmol/L of AUY922 and harvested at the indicated time intervals. Cell lysates were prepared from AUY922-untreated and -treated cells and immunoblot analyses were carried out for p-ATR, ATR, p-CHK1, CHK1, γ-H2AX, and ATM. The expression levels of β-actin in the lysates served as the loading control.

Treatment with AUY922 induces proteasomal degradation of ATR

Next, we determined whether treatment with AUY922 mediates depletion of ATR by first disrupting the binding of ATR to hsp90, and then promoting the polyubiquitylation and proteasomal degradation of ATR. HeLa cells expressing green fluorescent protein (GFP)-tagged CHK1 were treated with AUY922 for 16 hours, and hsp90 was immunoprecipitated with anti-hsp90 antibody, followed by immunoblot analysis with anti-ATR or anti-GFP antibody. AUY922 treatment reduced the binding of hsp90 to ATR (Fig. 4A, left). It also reduced the chaperone association of CHK1 with hsp90, seen as decreased binding of GFP-tagged CHK1 to hsp90. Reverse IP with anti-ATR antibody also showed that AUY922 treatment reduced the binding of ATR with hsp90 as well as with CHK1 (Fig. 4A, left). As has been shown for other hsp90 client proteins, this was concomitantly associated with increased binding of ATR to hsp70 (Fig. 4A; refs. 1, 17, 18, 33). Additionally, AUY922-mediated disruption of the binding of ATR with hsp90 was accompanied with an increase in polyubiquitylated ATR and other associated proteins in the immunoprecipitate with anti-ATR antibody (Fig. 4B). Treatment with the proteasome inhibitor bortezomib also increased the levels of polyubiquitylated proteins in the immunoprecipitates with anti-ATR antibody, and cotreatment with AUY922 and bortezomib further augmented the levels of polyubiquitylated proteins (Fig. 4B). However, cotreatment with bortezomib and AUY922, by blocking proteasomal degradation, restored the levels of ATR, p-ATR, p-CHK1, and CHK1 that had declined following treatment with AUY922 alone (Fig. 4C). Conversely, AUY922-induced γ-H2AX levels were partially reduced following cotreatment with bortezomib. Additionally, immunofluorescent analyses with anti-ubiquitin, anti-ATR, and DAPI staining also confirmed the restoration of the levels of ATR, following treatment with AUY922 and bortezomib (Fig. 4D).

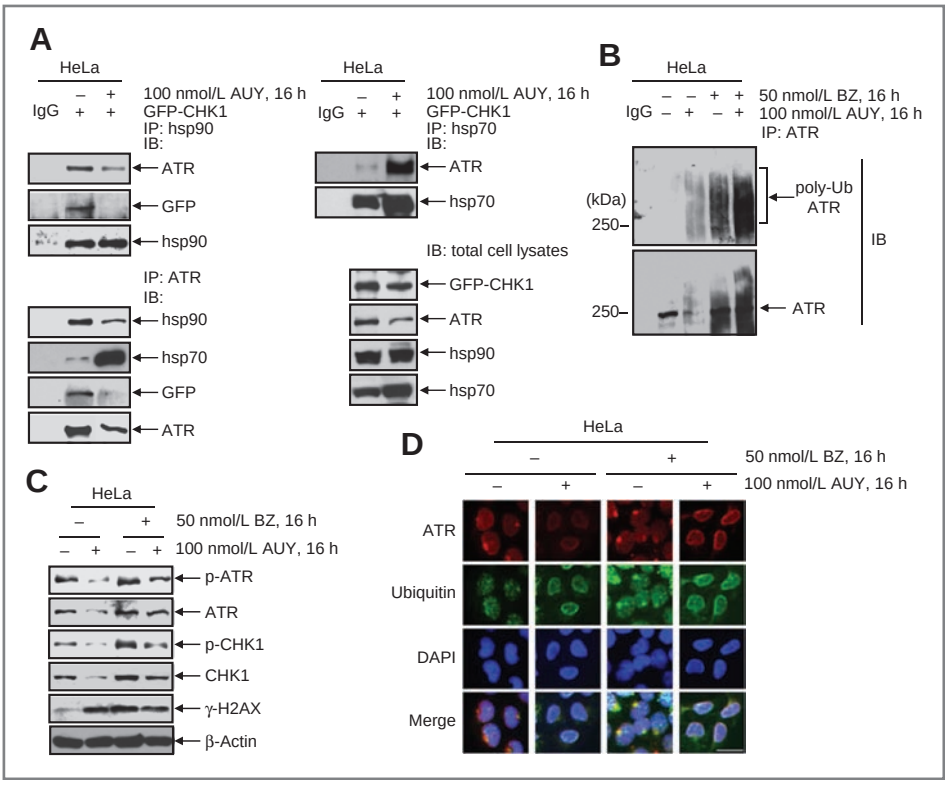

Figure 4. Treatment with AUY922 (AUY) induces proteasomal degradation of ATR in HeLa cells. A, HeLa cells with ectopic overexpression of GFP–CHK1 were treated with 100 nmol/L AUY for 16 hours. Following this, total cell lysates were prepared and hsp90, hsp70, and ATR were immunoprecipitated. Immunoblot analyses were carried out for CHK1, ATR, hsp70, or hsp90α on the immunoprecipitates. Alternatively, immunoblot analyses were carried out on the total cell lysates. The expression levels of β-actin in the cell lysates served as the loading control. B, HeLa cells were treated with AUY and/or bortezomib, as indicated, for 16 hours. At the end of treatment, cell lysates were prepared and ATR was immunoprecipitated. Immunoblot analyses were carried out for polyubiquitin or ATR. C, HeLa cells were treated with AUY and/or bortezomib, as indicated, for 16 hours. Following this, cell lysates were prepared and immunoblot analyses were carried out for p-ATR, ATR, p-CHK1, CHK1, and γ-H2AX. The expression levels of β-actin in the lysates served as the loading control. D, HeLa cells were plated on a chamber slide and cultured overnight at 37°C. The next day, cells were treated with the indicated concentrations of bortezomib and/or AUY for 16 hours. Cells were stained with anti-ATR and anti-ubiquitin antibodies and imaged by confocal microscopy. Representative images from 3 independent experiments are shown. Original magnification, ×40. Scale bar, 10 μm. IgG, immunoglobulin G; BZ, bortezomib.

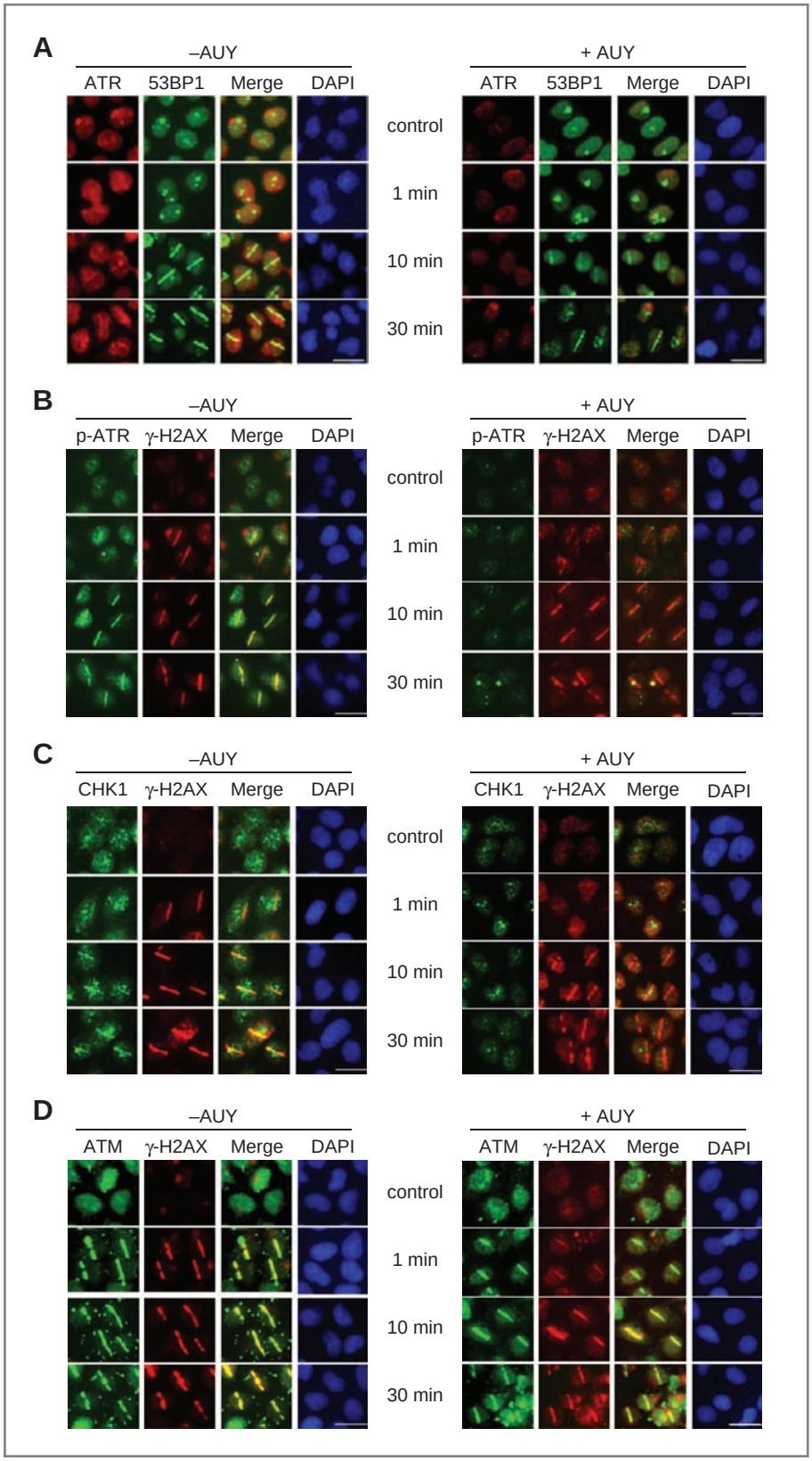

Figure 5. Treatment with AUY922 (AUY) inhibits localization of p-ATR, ATR, CHK1, and 53BP1 to sites of DNA damage. A–D, HeLa cells were treated with 100 nmol/L AUY for 16 hours and exposed to a laser microbeam (800 nm) along linear tracks. At the indicated times following laser exposure (1–30 minutes), cells were fixed and immunostained with anti-ATR and anti-53BP1 (A), anti–p-ATR and anti–γ-H2AX (B), anti-CHK1 and anti–γ-H2AX (C), or anti-ATM and anti–γ-H2AX (D) and imaged by confocal microscopy. Cell nuclei were stained with DAPI. Representative images from 3 independent experiments are shown. Original magnification, ×40. Scale bar, 10 μm.

Treatment with AUY922 inhibits localization of p-ATR, ATR, CHK1, and 53BP1 to sites of DNA damage

We next assessed the effect of AUY922 on the localization of ATR and other DDR proteins involved in DDR and repair to sites of DNA damage. HeLa cells were treated with 100 nmol/L AUY922 for 16 hours followed by exposure to 800 nm laser irradiation known to induce DNA DSBs. As shown in Fig. 5A and B, following laser irradiation, ATR and p-ATR accumulated at the sites of laser-induced DNA damage and colocalized with γ-H2AX. However, the accumulation of ATR and p-ATR, and colocalization with γ-H2AX, was inhibited by treatment with AUY922 (Fig. 5A and B). Previous reports have highlighted the role of p53BP1 in DNA damage checkpoint signals and in the recruitment of repair and signaling proteins to the sites of DNA damage following exposure to IR (4, 36). Consistent with this, we also observed the accumulation of ATR, p53BP1, and γ-H2AX at sites of DNA damage (Fig. 5A). AUY922 treatment inhibited the localization of p53BP1 and its colocalization with ATR at the sites of DNA damage (Fig. 5A). In contrast, AUY922 treatment increased γ-H2AX accumulation at the DNA damage sites. However, compared with the untreated control cells, AUY922 treatment attenuated the levels and colocalization of p-ATR with γ-H2AX (Fig. 5B). Similarly, AUY922 treatment significantly inhibited CHK1 accumulation and colocalization with γ-H2AX at the sites of laser-induced DNA damage (Fig. 5C). These studies also showed that compared with ATR, ATM accumulated at a rate faster than ATR at the sites of laser-induced DNA damage, but AUY922 treatment did not inhibit ATM accumulation (Fig. 5D).

Depletion of ATR by shRNA enhances sensitivity of cancer cells to IR, but not to AUY922

Next, we determined whether genetic knockdown of ATR would have a similar effect as AUY922 treatment on p-CHK1, γ-H2AX, cell cycle, apoptosis, and clonogenic survival. Figure 6A shows that shRNA-mediated knockdown of ATR depleted the levels of ATR, p-ATR, and p-CHK1, but increased γ-H2AX levels in HeLa cells. ATR knockdown also attenuated IR-mediated increase in p-ATR and p-CHK1 but augmented IR-induced γ-H2AX levels in HeLa cells (Fig. 6A). ATR knockdown did not

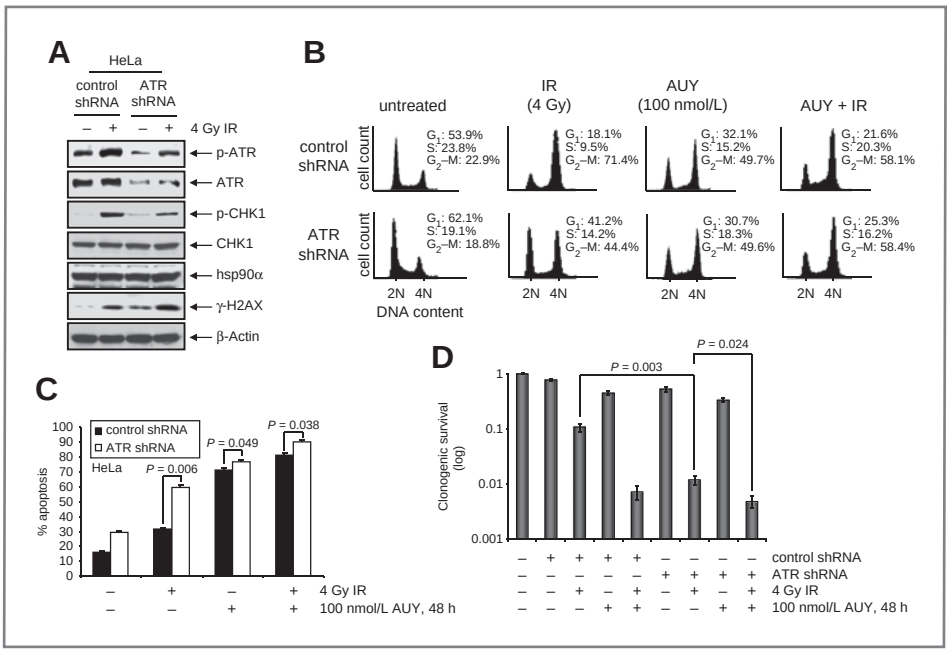

Figure 6. Depletion of ATR by shRNA enhances sensitivity of cancer cells to IR, but not to AUY922 (AUY). A, HeLa cells were transfected with control or ATR shRNA constructs and incubated for 48 hours. Following this, cells were exposed to 4 Gy of IR and incubated an additional 8 hours. Cell lysates were prepared and immunoblot analyses were carried out for p-ATR, ATR, p-CHK1, CHK1, hsp90α, and γ-H2AX. The expression levels of β-actin in the lysates served as the loading control. B, HeLa cells were transfected with control or ATR shRNA and incubated for 48 hours. Then, cells were treated with 100 nmol/L AUY and/or 4 Gy of IR (irradiation was administered 8 hours before the end of 16-hour AUY treatment) as indicated. After treatment, cells were fixed and stained with propidium iodide. Cell-cycle analyses were carried out by flow cytometry. Values represent the mean of 3 independent experiments. C, HeLa cells were transfected with control or ATR shRNA and incubated for 48 hours. Transfected cells were treated with 100 nmol/L AUY and/or 4 Gy of IR (irradiation was administered 8 hours before the end of 48-hour AUY treatment) as indicated. Then, cells were stained with Annexin V and propidium iodide and the percentages of apoptotic cells were determined by flow cytometry. Columns represent the mean of 3 independent experiments; bars represent the SEM. D, HeLa cells were transfected with control or ATR shRNA and incubated for 48 hours. Transfected cells were treated with 100 nmol/L of AUY for 16 hours. Following this, AUY-treated cells were either plated or exposed to 4 Gy of IR and plated for colony formation assay. Columns represent the log mean colony growth on day 10 compared with untreated control cells; bars represent the SEM.

affect the total levels of either CHK1 or hsp90 (Fig. 6A). As shown in Fig. 6B, knockdown of ATR, while increasing IR-induced G_1 accumulation inhibited the accumulation of IR-treated HeLa cells in the G_2–M phase of the cells cycle. Treatment with AUY922 also increased the accumulation of control HeLa cells or HeLa cells with ATR knockdown into the G_2–M phase of the cell cycle (Fig. 6B). Moreover, AUY922 treatment further augmented G_2–M accumulation of HeLa cells with knockdown of ATR following exposure to IR (Fig. 6B). We next determined the effects of pretreatment with AUY922 on IR-induced G_2–M accumulation and the levels of histone H3 p-S10 in HeLa cells. As presented in the Supplementary Fig. S3, pretreatment with AUY922 markedly enhanced IR-induced G_2–M accumulation and the levels of H3 p-S10 in HeLa cells.

We next determined whether the depletion of ATR augments AUY922 and/or IR-induced DNA damage and whether this is mostly restricted to the G_2–M phase of the cell cycle. We also determined the effects of ATR knockdown on IR- and/or AUY922-induced apoptosis in HeLa cells, and the effect of the depletion of ATR by shRNA on AUY922- and/or IR-induced γ-H2AX accumulation in HeLa cells. Compared with the cells transfected with the control nontargeted shRNA, we observed further augmentation of AUY922 and/or IR-induced γ-H2AX accumulation in HeLa cells showing a marked depletion of ATR by shRNA (Supplementary Fig. 4A and B). HeLa cells with knockdown of ATR were also significantly more sensitive to IR- and/or AUY922-induced apoptosis (Fig. 6C). Additionally, compared with the control, ATR knockdown by shRNA significantly enhanced IR-mediated loss of clonogenic survival of HeLa cells (Fig. 6D). Cotreatment with AUY922 further enhanced the IR-mediated loss of clonogenic survival of HeLa cell with knockdown of ATR (Fig. 6D). These results show that similar to the depletion of ATR by AUY922, ATR knockdown by shRNA also increases IR-mediated growth inhibition and apoptosis in cancer cells.

Treatment with AUY922 depletes ATR and CHK1 in nonproliferating cells

We next determined whether AUY922-mediated depletion of ATR and CHK1 is due to its effects on cell-cycle status. MCF-7 cells were cultured in serum-depleted media (0.5% FBS) for 24 to 72 hours to induce growth arrest and the effects on ATR and CHK1 expression levels were determined. As shown in Fig. 7A, MCF-7 cells were arrested in G_0–G_1 phase after serum starvation. Figure 7B shows that serum starvation induced G_0–G_1 arrest and resulted in only a modest decline in the levels of ATR and CHK1. Similar modest effect of serum starvation was also seen on DNA-PKcs and mTOR levels. Further, treatment with AUY922 induced significant decline in ATR and CHK1 levels, while inducing only a modest decline in the levels of DNA-PKcs and mTOR (Fig. 7B). During exposure of

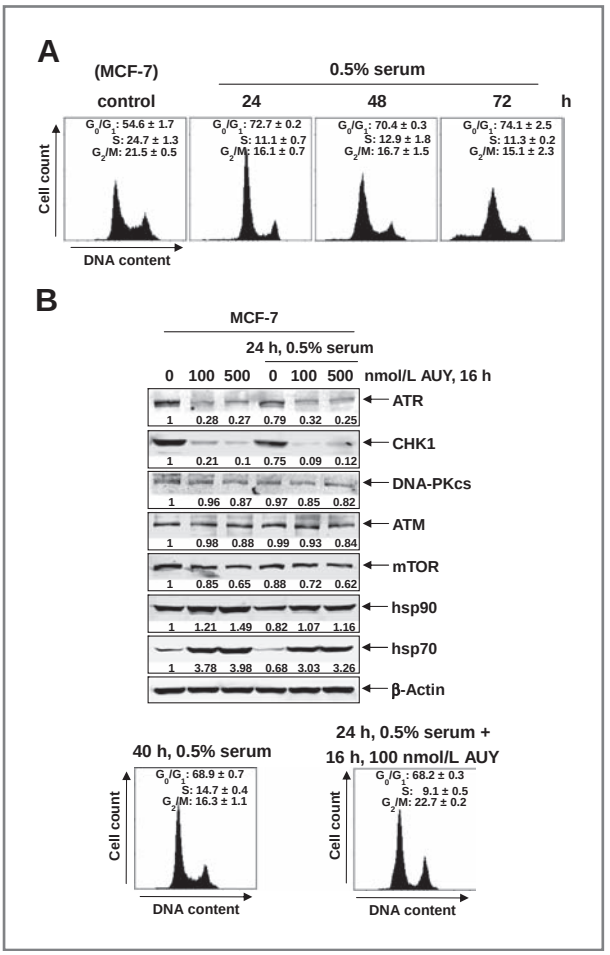

Figure 7. Treatment with AUY922 (AUY) induces depletion of ATR and CHK1 in nonproliferating cells. A, MCF-7 cells were cultured in 0.5% serum containing medium without or with 100 nmol/L of AUY for the indicated times. Then, cells were fixed, stained with propidium iodide, and cell-cycle analyses were carried out by flow cytometry. B, MCF-7 cells were cultured in 0.5% serum containing medium for 24 hours and treated with the indicated concentrations of AUY for 16 hours. Following this, total cell lysates were prepared and immunoblot analyses were carried out for ATR, CHK1, DNA-PKcs, ATM, mTOR, hsp90, and hsp70. The expression levels of β-actin in the lysates served as the loading control.

MCF7 cells to AUY922, no further changes in G_0–G_1 accumulation were observed (Fig. 7B). These findings show that AUY922-mediated depletion of ATR and CHK1 is not because of its effects on cell-cycle status.

Discussion

Although previous studies have highlighted CHK1 as a client protein of hsp90, we show here for the first time that ATR, which is upstream to CHK1 in the DDR signaling, also exhibits chaperone association with hsp90. This is supported by the observation that treatment with the hsp90 inhibitor AUY922 disrupts the binding of ATR to hsp90, promotes the shift in binding of ATR to hsp70 and induces polyubiquitylation of ATR,

thereby directing ATR to proteasomal degradation. Consistent with this, although treatment with AUY922 decreased the half-life of ATR, cotreatment with bortezomib restored the levels of ATR. Furthermore, AUY922 treatment did not decrease the mRNA levels of ATR, supporting the conclusion that the effect of AUY922 on ATR is largely posttranscriptional, resulting in attenuation of ATR levels. Our findings also show that the effect of AUY922 on ATR levels is dose-dependent, as well as dependent on the exposure interval to AUY922. Similar effect on ATR levels was observed following exposure to the geldanamycin analogue 17-AAG. Importantly, the levels of CHK1 and ATR were restored within 24 to 48 hours after AUY922 withdrawal. This suggests that the biologic consequences of hsp90 inhibition by AUY922, resulting from the depletion of the client proteins, would also abate over time. This finding has considerable implications for the clinical efficacy of hsp90 inhibitors such as AUY922 and 17-AAG (tanespimycin), because these agents are currently under clinical investigation (37, 38). Our studies also clearly show that exposure to hsp90 inhibitor did not deplete ATM levels, suggesting that not all PIKK family members exhibit chaperone association with hsp90. The mechanism underlying this difference between ATR versus ATM for chaperone dependence on hsp90 remains to be elucidated (17, 18).

As a master regulator of DDR, ATR is activated by various types of DNA damage (3, 4). When activated by IR-induced DNA damage, ATR phosphorylates and activates CHK1 and other DDR proteins, resulting in cell-cycle arrest (3, 4, 7). Consistent with this, knockdown of ATR by shRNA increased the accumulation of HeLa cells in the G_1 phase of the cell cycle. ATR knockdown also increased IR-induced G_1 arrest but reduced the G_2–M phase accumulation of HeLa cells in the cell cycle. In addition to its role in cell-cycle checkpoint, ATR also regulates DNA repair by inducing phosphorylation and causing intracellular redistribution of DNA repair proteins (4, 39). Among the repair proteins phosphorylated by ATR are the BRCA1, WRN, BLM, FANCD2, and XPA proteins, which are involved in DNA repair by homologous recombination and nucleotide excision repair (4, 39, 40–43). Therefore, ATR-mediated signaling also regulates the repair of several types of DNA lesions. Consistent with this, findings presented here show that ATR knockdown by shRNA enhanced IR-induced DNA fragments, as shown here by increased tail moment in the comet assay. This was also highlighted by an increase in IR-induced accumulation of γ-H2AX levels in HeLa cells following ATR knockdown. Taken together, these findings show that ATR knockdown significantly increases IR-induced apoptosis and loss of clonogenic survival of cancer cells.

Following the discovery that geldanamycin and its analogues inhibit hsp90 chaperone function and deplete the levels of a large number of hsp90 client proteins that are involved in conferring the key hallmarks of malignancy and mediating DDR in transformed cells, hsp90 inhibitors have been shown to sensitize cancer cells to genotoxic agents including IR (17, 18). As an hsp90 inhibitor, treatment with AUY922 depleted the levels of ATR and CHK1. We also observed that in the cells treated with AUY922, not only the recruitment of p53BP1 but also its colocalization with ATR at the sites of laser-induced DNA damage was inhibited, although it is not clear what accounts for the inhibition of 53BP1 recruitment to sites of DNA damage in AUY922-treated cells. AUY922 would also reduce the levels of other cell-cycle regulatory kinases, for example, CDK4 and WEE1, which are hsp90 client proteins (17, 18). Also, AUY922 would undermine the chaperone association of hsp90 with other proteins involved in DNA damage repair, including the MRE11–RAD50–NBS1 (MRN) complex, BRCA1 and 2, and FANCD2 (17, 18, 20, 23, 40). Therefore, AUY922-mediated hsp90 inhibition would also broadly undermine DDR and DNA repair, although AUY922 may have a somewhat different effect than specific knockdown of ATR by shRNA on cell-cycle status in the untreated and IR-treated cancer cells. Accordingly, treatment with AUY922, unlike ATR knockdown by shRNA, reduced the percentage of HeLa cells in the G_1 phase while causing their G_2–M phase accumulation. However, similar to the knockdown of ATR by shRNA, AUY922 treatment also increased IR-induced G_2–M accumulation. Additionally, following exposure to IR, treatment with AUY922 not only increased DNA fragmentation but also caused the persistence of damaged DNA fragments, as shown by increased tail moment in the comet assay. Clearly, the inhibitory effect of AUY922 on IR-induced DDR does not involve ATM, because AUY922 treatment did not alter ATM levels. Recently, pan-histone deacetylase inhibitors, for example, vorinostat and panobinostat, have been shown to induce hyperacetylation of hsp90, which inhibits its chaperone association with hsp90 client proteins leading to depletion of the client proteins (35, 44). Accordingly, cotreatment with these agents has also been shown to exert radiosensitizing effects on cancer cells (34).

Collectively, findings presented here further contribute to our understanding of how treatment with hsp90 inhibitor such as AUY922 sensitizes cancer cells to IR-induced apoptosis and loss of clonogenic survival. These findings underscore that the depletion of ATR-CHK1–induced DDR signaling is an important mechanism of radiosensitization induced by hsp90 inhibitors. Recent studies have highlighted that BRCA1-deficient cancer cells with impaired homology-dependent repair are especially sensitive to agents that target and inhibit the nucleotide excision repair alone and in combination with genotoxic agents (45, 46). Findings presented here also support further evaluation of targeting ATR-CHK1–induced DDR signaling in the genetic background of cancer cells in which the homology repair of DNA damage is compromised. Thus, targeting ATR-CHK1–

induced DDR signaling seems to be a promising target for anticancer drug development.

Disclosure of Potential Conflicts of Interest

No potential conflicts of interest were disclosed.

The costs of publication of this article were defrayed in part by the payment of page charges. This article must therefore be hereby marked *advertisement* in accordance with 18 U.S.C. Section 1734 solely to indicate this fact.

Received February 3, 2011; revised April 18, 2011; accepted May 8, 2011; published OnlineFirst May 12, 2011.

References

1. Shiloh Y. ATM and related protein kinases: safeguarding genome integrity. Nat Rev Cancer 2003;3:155–68.
2. Kastan MB, Bartek J. Cell-cycle checkpoints and cancer. Nature 2004;432:316–23.
3. Ciccia A, Elledge SJ. The DNA damage response: making it safe to play with knives. Mol Cell 2010;40:179–204.
4. Cimprich KA, Cortez D. ATR: an essential regulator of genome integrity. Nat Rev Mol Cell Biol 2008;9:616–27.
5. de Klein A, Muijtjens M, van Os R, Verhoeven Y, Smit B, Carr AM, et al. Targeted disruption of the cell-cycle checkpoint gene ATR leads to early embryonic lethality in mice. Curr Biol 2000;10:479–82.
6. Brown EJ, Baltimore D. ATR disruption leads to chromosomal fragmentation and early embryonic lethality. Genes Dev 2000;14:397–402.
7. Cortez D, Guntuku S, Qin J, Elledge SJ. ATR and ATRIP: partners in checkpoint signaling. Science 2001;294:1713–16.
8. Zou L, Liu D, Elledge SJ. Replication protein A-mediated recruitment and activation of Rad17 complexes. Proc Natl Acad Sci U S A 2003;100:13827–32.
9. Kumagai A, Lee J, Yoo HY, Dunphy WG. TopBP1 activates the ATR-ATRIP complex. Cell 2006;124:943–55.
10. Helt CE, Cliby WA, Keng PC, Bambara RA, O'Reilly MA. Ataxia telangiectasia mutated (ATM) and ATM and Rad3-related protein exhibit selective target specificities in response to different forms of DNA damage. J Biol Chem 2005;280:1186–92.
11. Sørensen CS, Syljuåsen RG, Falck J, Schroeder T, Rönnstrand L, Khanna KK, et al. Chk1 regulates the S phase checkpoint by coupling the physiological turnover and ionizing radiation-induced accelerated proteolysis of Cdc25A. Cancer Cell 2003;3:247–58.
12. Mailand N, Falck J, Lukas C, Syljuåsen RG, Welcker M, Bartek J, et al. Rapid destruction of human Cdc25A in response to DNA damage. Science 2000;288:1425–29.
13. Zhao H, Watkins JL, Piwnica-Worms H. Disruption of the checkpoint kinase 1/cell division cycle 25A pathway abrogates ionizing radiation-induced S and G2 checkpoints. Proc Natl Acad Sci U S A 2002;99:14795–14800.
14. Zhou BB, Bartek J. Targeting the checkpoint kinases: chemosensitization versus chemoprotection. Nat Rev Cancer 2004;4:216–25.
15. Takai H, Wang RC, Takai KK, Yang H, de Lange T. Tel2 rgulates the stability of PI3K-related protein kinases. Cell 2007;131:1248–59.
16. Takai H, Xie Y, de Lange T, Pavletich NP. Tel2 structure and function in the Hsp90-dependent maturation of mTOR and ATR complexes. Genes Dev 2010;24:2019–30.
17. Taipale M, Jarosz DF, Lindquist S. HSP90 at the hub of protein homeostasis: emerging mechanistic insights. Nat Rev Mol Cell Biol 2010;11:515–28.
18. Trepel J, Mollapour M, Giaccone G, Neckers L. Targeting the dynamic HSP90 complex in cancer. Nat Rev Cancer 2010;10:537–49.
19. Arlander SJ, Eapen AK, Vroman BT, McDonald RJ, Toft DO, Karnitz LM. Hsp90 Inhibition Depletes Chk1 and Sensitizes Tumor Cells to Replication Stress. J Biol Chem 2003;278:52572–77.
20. Dote H, Burgan WE, Camphausen K, Tofilon PJ. Inhibition of hsp90 compromises the DNA damage response to radiation. Cancer Res 2006;66:9211–20.
21. Noguchi M, Yu D, Hirayama R, Ninomiya Y, Sekine E, Kubota N, et al. Inhibition of homologous recombination repair in irradiated tumor cells pretreated with Hsp90 inhibitor 17-allylamino-17-demethoxygeldanamycin. Biochem Biophys Res Commun 2006;351:658–63.
22. Sekimoto T, Oda T, Pozo FM, Murakumo Y, Masutani C, Hanaoka F, et al. The molecular chaperone hsp90 regulates accumulation of DNA polymerase η at replication stalling sites in UV-irradiated cells. Mol Cell 2010;37:79–89.
23. Oda T, Hayano T, Miyaso H, Takahashi N, Yamashita T. Hsp90 regulates the Fanconi anemia DNA damage response pathway. Blood 2007;109:5016–26.
24. Jensen MR, Schoepfer J, Radimerski T, Massey A, Guy CT, Brueggen J, et al. NVP-AUY922: a small molecule HSP90 inhibitor with potent antitumor activity in preclinical breast cancer models. Breast Cancer Res 2008;10:R33.
25. Eccles SA, Massey A, Raynaud FI, Sharp SY, Box G, Valenti M, et al. NVP-AUY922: a novel heat shock protein 90 inhibitor active against xenograft tumor growth, angiogenesis, and metastasis. Cancer Res 2008;68:2850–60.
26. Gaspar N, Sharp SY, Eccles SA, Gowan S, Popov S, Jones C, et al. Mechanistic evaluation of the novel HSP90 inhibitor NVP-AUY922 in adult and pediatric glioblastoma. Mol Cancer Ther 2010;9:1219–33.
27. Bisht KS, Bradbury CM, Mattson D, Kaushal A, Sowers A, Markovina S, et al. Geldanamycin and 17-allylamino-17-demethoxygeldanamycin potentiate the in vitro and in vivo radiation response of cervical tumor cells via the heat shock protein 90-mediated intracellular signaling and cytotoxicity. Cancer Res 2003;63:8984–95.
28. Stingl L, Stühmer T, Chatterjee M, Jensen MR, Flentje M, Djuzenova CS. Novel HSP90 inhibitors, NVP-AUY922 and NVP-BEP800, radiosensitise tumour cells through cell-cycle impairment, increased DNA damage and repair protraction. Br J Cancer 2010;102:1578–91.
29. Franken NA, Rodermond HM, Stap J, Haveman J, van Bree C. Clonogenic assay of cells in vitro. Nat Protoc 2006;1:2315–9.
30. Rao R, Nalluri S, Kolhe R, Yang Y, Fiskus W, Chen J, et al. Treatment with panobinostat induces glucose-regulated protein 78 acetylation and endoplasmic reticulum stress in breast cancer cells. Mol Cancer Ther 2010;9:942–52.
31. Mari PO, Florea BI, Persengiev SP, Verkaik NS, Brüggenwirth HT, Modesti M, et al. Dynamic assembly of end-joining complexes requires interaction between Ku70/80 and XRCC4. Proc Natl Acad Sci U S A 2006;103:18597–602.
32. Rao R, Nalluri S, Fiskus W, Savoie A, Buckley KM, Ha K, et al. Role of CAAT/enhancer binding protein homologous protein in panobinostat-mediated potentiation of bortezomib-induced lethal endoplasmic reticulum stress in mantle cell lymphoma cells. Clin Cancer Res 2010;16:4742–54.
33. Fiskus W, Wang Y, Joshi R, Rao R, Yang Y, Chen J, et al. Cotreatment with vorinostat enhances activity of MK-0457 (VX-680) against acute and chronic myelogenous leukemia cells. Clin Cancer Res 2008;14:6106–15.
34. Geng L, Cuneo KC, Fu A, Tu T, Atadja PW, Hallahan DE. Histone deacetylase (HDAC) inhibitor LBH589 increases duration of gamma-H2AX foci and confines HDAC4 to the cytoplasm in irradiated non-small cell lung cancer. Cancer Res 2006;66:11298–304.
35. Yang Y, Rao R, Shen J, Tang Y, Fiskus W, Nechtman J, et al. Role of acetylation and extracellular location of heat shock protein 90alpha in tumor cell invasion. Cancer Res 2008;68:4833–42.
36. Wang B, Matsuoka S, Carpenter PB, Elledge SJ. 53BP1, a mediator of the DNA damage checkpoint. Science 2002;298:1435–8.
37. Modi S, Stopeck AT, Gordon MS, Mendelson D, Solit DB, Bagatell R, et al. Combination of trastuzumab and tanespimycin (17-AAG,

KOS-953) is safe and active in trastuzumab-refractory HER-2 overexpressing breast cancer: a phase I dose-escalation study. J Clin Oncol 2007;25:5410–7.
38. Sessa C, Sharma SK, Britten CD, Vogelzang NJ, Bhalla K, Mita MM,, et al. A phase I dose escalation study of AUY922, a novel HSP90 inhibitor, in patients with advanced solid malignancies. J Clin Oncol 2009;27:15s.
39. Wu X, Shell SM, Liu Y, Zou Y. ATR-dependent checkpoint modulates XPA nuclear import in response to UV irradiation. Oncogene 2007;26:757–64.
40. Tibbetts RS, Cortez D, Brumbaugh KM, Scully R, Livingston D, Elledge SJ, et al. Functional interactions between BRCA1 and the checkpoint kinase ATR during genotoxic stress. Genes Dev 2000; 14:2989–3002.
41. Pichierri P, Rosselli F, Franchitto A. Werner's syndrome protein is phosphorylated in an ATR/ATM-dependent manner following replication arrest and DNA damage induced during the S phase of the cell cycle. Oncogene 2003;22:1491–500.
42. Davies SL, North PS, Dart A, Lakin ND, Hickson ID. Phosphorylation of the Bloom's syndrome helicase and its role in recovery from S-phase arrest. Mol Cell Biol 2004;24:1279–91.
43. Andreassen PR, D'Andrea AD, Taniguchi T. ATR couples FANCD2 monoubiquitination to the DNA-damage response. Genes Dev 2004;18:1958–63.
44. Rao R, Fiskus W, Yang Y, Lee P, Joshi R, Fernandez P, et al. HDAC6 inhibition enhances 17-AAG–mediated abrogation of hsp90 chaperone function in human leukemia cells. Blood 2008;112:1886–93.
45. Banerjee S, Kaye SB, Ashworth A. Making the best of PARP inhibitors in ovarian cancer. Nat Rev Clin Oncol 2010;7:508–19.
46. Rowe BP, Glazer PM. Emergence of rationally designed therapeutic strategies for breast cancer targeting DNA repair mechanisms. Breast Cancer Res 2010;12:203.